Acta Crystallographica Section D
Biological Crystallography
ISSN 1399-0047

Stealth carriers for low-resolution structure determination of membrane proteins in solution

Selma Maric,[a] Nicholas Skar-Gislinge,[a] Søren Midtgaard,[a] Mikkel B. Thygesen,[b] Jürgen Schiller,[c] Henrich Frielinghaus,[d] Martine Moulin,[e,f] Michael Haertlein,[e] V. Trevor Forsyth,[e,f] Thomas Günther Pomorski[g] and Lise Arleth[a]*

[a]Niels Bohr Institute, University of Copenhagen, Universitetsparken 5, 2100 Copenhagen, Denmark, [b]CARB Centre, Department of Chemistry, University of Copenhagen, Thorvaldsensvej 40, 1871 Frederiksberg C, Denmark, [c]Institut für Medizinische Physik und Biophysik, Medizinische Fakultät, Universität Leipzig, Härtelstrasse 16-18, 04107 Leipzig, Germany, [d]Forschungszentrum Jülich GmbH, Jülich Centre for Neutron Scattering, TUM FRM-2, Lichtenbergstrasse 1, 85747 Garching, Germany, [e]Life Sciences Group, Institut Laue–Langevin, 6 Rue Jules Horowitz, 38042 Grenoble, France, [f]EPSAM/ISTM, Keele University, Staffordshire ST5 5BG, England, and [g]Center for Membrane Pumps in Cells and Disease, Department of Plant and Environmental Sciences, University of Copenhagen, Thorvaldsensvej 40, Frederiksberg C, Denmark

Correspondence e-mail: arleth@nbi.ku.dk

Received 14 June 2013
Accepted 7 October 2013

Structural studies of membrane proteins remain a great experimental challenge. Functional reconstitution into artificial nanoscale bilayer disc carriers that mimic the native bilayer environment allows the handling of membrane proteins in solution. This enables the use of small-angle scattering techniques for fast and reliable structural analysis. The difficulty with this approach is that the carrier discs contribute to the measured scattering intensity in a highly nontrivial fashion, making subsequent data analysis challenging. Here, an elegant solution to circumvent the intrinsic complexity brought about by the presence of the carrier disc is presented. In combination with small-angle neutron scattering (SANS) and the D_2O/H_2O-based solvent contrast-variation method, it is demonstrated that it is possible to prepare specifically deuterated carriers that become invisible to neutrons in 100% D_2O at the length scales relevant to SANS. These 'stealth' carrier discs may be used as a general platform for low-resolution structural studies of membrane proteins using well established data-analysis tools originally developed for soluble proteins.

1. Introduction

Despite significant recent breakthroughs in the field of membrane-protein X-ray crystallography (Rasmussen *et al.*, 2007; Cherezov *et al.*, 2007; Rosenbaum *et al.*, 2007; Rasmussen, Choi *et al.*, 2011; Rasmussen, DeVree *et al.*, 2011), including the award of the 2012 Nobel Prize in Chemistry to Lefkowitz and Kobilka for their contributions toward the understanding of G-protein-coupled receptor systems (Roth & Marshall, 2012), there is still an important lack of structural insight into membrane proteins and their complexes (Bhattacharya, 2009; White, 2009). This is most clearly illustrated by the extremely low number of unique membrane-protein structures available in the Protein Data Bank compared with their 30% prevalence in the human proteome (Fagerberg *et al.*, 2010) and their importance as targets for about 50% of all current drugs (Terstappen & Reggiani, 2001; Xia *et al.*, 2006). Of the 80 000 available protein structures to date, only 400 represent membrane proteins, with around a dozen of these being human membrane-protein structures (Baker, 2010). This creates an obvious need for alternative methods that complement crystallography, nuclear magnetic resonance (NMR) and (cryo) transmission electron microscopy (TEM) approaches for this important class of drug targets.

Over the last decade, small-angle X-ray scattering (SAXS) and small-angle neutron scattering (SANS) have become increasingly important methods in structural studies of water-

soluble protein systems (Jacques & Trewhella, 2010; Petoukhov & Svergun, 2012; Blanchet & Svergun, 2013; Rambo & Tainer, 2013). Recent developments of these techniques at synchrotron radiation and neutron beam sources, in combination with sophisticated sample-preparation procedures and better, more robust and more general data-analysis software tools (Konarev *et al.*, 2006; Jacques *et al.*, 2012), makes small-angle scattering (SAS) an increasingly important tool for the study of biomolecular systems. While SAS only has a structural resolution of the order of 10 Å, which does not provide information at the sorts of length scales accessible to protein crystallography or NMR, it has the significant advantage of allowing rapid protein studies in solution and native-like environments. Furthermore, the solution properties may easily be varied in a way that allows parametric studies such as those relating to temperature, buffer conditions and pH (Round *et al.*, 2008; Toft *et al.*, 2008; Hura *et al.*, 2009). This is powerful for studies of structural flexibility, which is of central importance in protein function, self-assembly and dynamic metabolon formation. Previously, SAS studies have been carried out using membrane proteins stabilized with detergent micelles or liposomes (Chan & Boxer, 2007) or using more advanced systems such as amphipoles (Pocanschi *et al.*, 2006) or nanodiscs (Nath *et al.*, 2007). The requirements for sample volumes and sample concentrations have been brought down to about 10–20 µl at protein concentrations of a few milligrams per millilitre for SAXS and 100–300 µl at a similar protein concentration for SANS (Jacques & Trewhella, 2010). This is compatible with what is typically attainable for many membrane-protein systems (Midgett & Madden, 2007; Tate, 2010). Nevertheless, SAS has to date only provided limited structural knowledge on membrane proteins despite a few breakthroughs (Hunt *et al.*, 1997; Berthaud *et al.*, 2012; Calcutta *et al.*, 2012), mainly because it is difficult to extract the low-resolution structure of the membrane protein alone from SAS data measured on a complex multi-component system.

We have now developed a versatile and robust methodology to circumvent this intrinsic complexity through the use of the well tested and structurally well defined nanodisc system for membrane-protein reconstitution (Bayburt *et al.*, 2002; Nath *et al.*, 2007; Ritchie *et al.*, 2009). In combination with the D_2O/H_2O-based contrast-variation method in neutron scattering (Jacrot, 1976), we demonstrate that it is possible to control the *Escherichia coli*-based biosynthesis of deuterated phosphatidylcholines as well as the expression of membrane-scaffolding proteins to prepare specifically deuterated analogues of the nanodisc which give a minimal contribution to the neutron scattering data when used in 100% D_2O. In this context, a particular challenge has been to control the deuteration levels in the phospholipid head and tail groups, respectively. The stealth discs produced in this way should be generally usable in low-resolution structural studes of many membrane proteins and their complexes in solution. The analysis of SANS data for this platform is greatly simplified and allows the application of existing data analysis tools that are already available for soluble proteins.

2. Materials and methods

2.1. Expression and purification of deuterated membrane-scaffold protein MSP1D1 (D-MSP1S1)

D-MSP1D1 was overexpressed in *E. coli* strain BL21 (DE3) using a pET-28a vector after an initial adaptation process of the strain to minimal deuterated medium as described previously (Artero *et al.*, 2005). High cell-density cultures were grown in 85% deuterated minimal medium containing glycerol as a carbon source (Rochel *et al.*, 2011). The protein was purified according to a modified version of the established method (Ritchie *et al.*, 2009). All sets of protein lipid deuteration were carried out in collaboration with the Deuteration Laboratory PSB platform within the Life Sciences Group at the Institut Laue–Langevin (ILL), Grenoble, France.

2.2. Production and purification of deuterated phosphatidylcholine

E. coli strain AL95 carrying the plasmid pAC-PCSlp-Sp-Gm allowing the biosynthesis of phosphatidylcholine (PC; Bogdanov *et al.*, 2010) was adapted to minimal deuterated medium according to previously established procedures (Artero *et al.*, 2005). Selective deuteration of PC with the relevant scattering-length density was achieved by amplifying the adapted starting culture in ∼100% deuterated minimal medium (Artero *et al.*, 2005) containing 0.2% arabinose (Sigma–Aldrich), 5% deuterated glycerol (1,1,2,3,3-d_5, 99%; Eurisotop) and 2 m*M* deuterated choline chloride (trimethyl-d_9, 98%; Eurisotop). To obtain partial deuteration, hydrogenated glycerol, as well as hydrogenated choline, were used instead. After cultivation at 310 K for 24 h, the cells were harvested by centrifugation and the total cellular lipids were extracted by the method of Bligh & Dyer (1959). Lipid extracts were separated into individual phospholipids using silica-gel chromatography with varying ratios of chloroform and methanol [9:1 (0.2 l), 4:1 (0.2 l), 1:1 (0.2 l), 1:4 (0.2 l) and 100% methanol (0.3 l)].

2.3. Phospholipid analysis

Phospholipid species were separated by thin-layer chromatography (TLC) using chloroform/ethanol/water/triethylamine [30:35:7:35(*v*:*v*:*v*:*v*)] and identified by comparison with known standards chromatographed on the same plate after staining with primuline [5 mg primuline in 100 ml 80:20(*v*:*v*) acetone:water; White *et al.*, 1998]. For further analysis, lipid spots were scraped off and extracted three times with 100 µl chloroform/methanol/0.9% aqueous NaCl [1:1:1(*v*:*v*:*v*)]. The lipid concentration was quantified by determination of the total phosphorus as described previously (Rouser *et al.*, 1966).

2.4. MALDI–TOF mass spectrometry

The extracted lipids were analysed using matrix-assisted laser desorption/ionization time-of-flight (MALDI–TOF) mass spectrometry as described previously (Schiller *et al.*, 2004). The lipid fractions were independently pre-mixed in a

1:1(*v*:*v*) ratio with different matrix compounds [2,5-dihydroxybenzoic acid (DHB) and 9-aminoacridine (9-AA)] prior to deposition onto the MALDI target and were investigated by both positive and negative ion-mode MALDI–TOF MS on a Bruker Autoflex mass spectrometer (Bruker Daltonics; Petkovic *et al.*, 2001). The lipids were also analysed subsequent to PLA_2 digestion in order to determine the fatty-acyl composition, as described previously (Fuchs *et al.*, 2007).

2.5. NMR spectroscopy

The locations of the incorporated deuterium atoms in the lipid molecules were determined by ^{1}H NMR through comparison of 5% solutions of hydrogenated PC, of partially deuterated PC synthesized with hydrogenated glycerol and hydrogenated choline and of deuterated PC synthesized with deuterated glycerol and deuterated choline all achieved in *E. coli*. The lipids were dissolved in chloroform-d [99.96%, 0.03%(*v*:*v*) TMS as internal reference] and measured on a 300 MHz NMR spectrometer (Bruker).

2.6. Stealth carrier disc preparation

Liposomes were prepared by extrusion of the stealth PC lipids in D_2O buffer solution (20 m*M* Tris–HCl, 100 m*M* NaCl pH 7.5) through 100 nm polycarbonate filters (Avanti Polar Lipids Inc). Liposomes at different D_2O:H_2O ratios were achieved through dilution of the D_2O-based liposome stock preparation with an adequate amount of H_2O buffer solution (20 m*M* Tris–HCl, 100 m*M* NaCl pH 7.5). This allowed liposomes to be obtained at 60–100% D_2O for subsequent SANS measurements. The liposome size was confirmed through dynamic light scattering on a BI-200SM System (Brookhaven Instruments). Stealth nanodiscs were reconstituted using the deuterated version of MSP1D1 together with the deuterated stealth PC lipids through the previously described self-assembly-based procedure (Ritchie *et al.*, 2009). All SAXS measurements were performed in H_2O-based buffer. Prior to the SANS measurements, the H_2O-based buffer used in the initial nanodisc preparation was substituted for a 100% D_2O-based buffer solution using centrifugal spin-filters with a cutoff of 50 kDa (Millipore). To achieve the H_2O:D_2O ratios required for the subsequent SANS measurements (60–100% D_2O), the nanodisc stock solution in 100% D_2O was diluted with an adequate amount of H_2O buffer solution.

2.7. SANS contrast variation

All reported contrast-variation SANS data were collected at 25°C using the KWS1 instrument at the Forschungs-Neutronenquelle Heinz Maier-Leibnitz (FRMII) in Munich, while initial pilot data as well as the data from nanodiscs prepared with commercially available POPC (Avanti Polar Lipids Inc.) were obtained using the D11 instrument at the Institut Laue–Langevin (ILL), Grenoble. All reported measurements from FRMII were performed with 4.5 Å neutrons with a wavelength spread $\Delta\lambda/\lambda$ of 10% FWHM. A combination of two to three instrumental settings were used to obtain a sufficiently wide q-range: high q-values (0.035–0.45 Å^{-1}) were covered with a sample-to-detector distance of 1.5 m and a collimation length of 4 m. Intermediate q-values (0.0057–0.077 Å^{-1}) were covered with a sample-to-detector distance of 8 m and a collimation length of 8 m. Low q-values (0.0022–0.03 Å^{-1}) were covered with a sample-to-detector distance of 20 m and a collimation length of 20 m. Owing to the small size of the nanodiscs, these were only measured at high and intermediate q-values, while the liposomes, which have structural features ranging from the ∼40 Å bilayer thickness to the ∼1200 Å liposome diameter, had to be measured at all three settings. Absolute scale calibration was performed using a calibrated Plexiglas sample as an external reference and following the standard procedures at the facility. Radial averaging, background subtraction and absolute scale calibration to convert the data into scattering intensity $I(q)$ in units of cm^{-1} as a function of momentum transfer $q = 4\pi\sin\theta/\lambda$ (where θ is the half scattering angle and λ is the wavelength of the incoming beam) was carried out using the *QtiKWS* software (Pipich, 2007). Small resolution effects were present in the SANS data, mainly owing to the non-negligible wavelength spread of the incoming neutrons. These were taken into account in the subsequent model-based data analysis by smearing of the fit function with the calculated resolution function (Pedersen *et al.*, 1990). All samples were measured in flat rectangular Hellma quartz cells. The samples in 85–100% D_2O were measured in cells with a path length of 2 mm, whereas the samples in 60–80% D_2O were measured in cells with a path length of 1 mm in order to optimize the signal-to-noise ratio and to minimize incoherent background and multiple-scattering effects.

2.8. SAXS structural analysis

The nanodiscs were characterized by SAXS using the Bio-SAXS instrument BM29 at the European Synchrotron Radiation Facility (ESRF), Grenoble. All SAXS data were collected at 20°C at q-values ranging from 0.0040 to 0.45 Å^{-1} with $q = 4\pi\sin\theta/\lambda$ using the fixed instrument setup described for the now disassembled beamline ID14-3 (Pernot *et al.*, 2010), a predecessor of the current beamline. Data processing, including radial averaging, background subtraction and conversion of the data into $I(q)$ (units of cm^{-1}) was performed using the *ATSAS* package (Konarev *et al.*, 2006). Calibration of the scattering intensity into absolute units of cm^{-1} was performed using the forward scattering intensity of bovine serum albumin prepared at a concentration of 3.2 mg ml^{-1} as an external reference. Resolution effects were considered to be negligible owing to the very high monochromaticity of the incoming beam, a very small beam diameter and close to perfect collimation. The data were analysed using an established approach for the nanodisc system (Skar-Gislinge & Arleth, 2011; Skar-Gislinge *et al.*, 2010).

2.9. Determination of forward scattering intensity *I*(0)

For each contrast measurement, the forward scattering was estimated by the indirect Fourier transform method with overlap optimization and background correction (Glatter,

1977; Pedersen *et al.*, 1994) and by taking the resolution effects into account (Pedersen *et al.*, 1990). The absolute scaled data for the liposome and nanodisc samples were normalized by sample concentration and the match points were derived in the standard way (Stuhrmann, 1982) by fitting a second-order polynomial to the forward scattering plotted as a function of volume fraction of D_2O in the buffer solution.

2.10. Model calculation of liposomes

The theoretical scattering signal for D_{64}-POPC liposomes was calculated using the same approach and Fortran77 implementation of the analytical model as previously described in Andersen *et al.* (2011). However, to adapt the calculations to the D_{64}-POPC case, the following total lipid scattering lengths, b, and partial specific molecular volumes, ν, were applied: PC head group, $b = 6.0 \times 10^{-12}$ cm, $\nu = 319$ Å^3; PO tail group, $b = 6.4 \times 10^{-11}$ cm, $\nu = 927$ Å^3. The model calculations assume that the liposomes are measured on a background of 100% D_2O with a scattering length density of 6.38×10^{10} cm^{-2}. An average liposome radius of 500 Å in a Gaussian distribution with $\Delta\sigma/\sigma = 0.25$ was assumed, with a liposome bilayer thickness of 40 Å. This is an idealized model calculation which does not take into account incoherent background effects or other small effects that are typically present in the experimental situation and that contribute to the overall observed scattering.

2.11. Model calculation of protein scattering signal

The theoretical scattering signal for the epidermal growth factor receptor (EGFR) was based on a combination of available crystal structures (PDB entries 1ivo, 1nql, 2jwa, 1egf and 2gs6) which were assembled manually using *PyMOL* (v.1.5.0.4; Schrödinger) based on available structural information for the system (Montelione *et al.*, 1992; Ogiso *et al.*, 2002; Ferguson *et al.*, 2003; Zhang *et al.*, 2006; Bocharov *et al.*, 2008). Assuming one active dimer per nanodisc, the scattering data were then calculated using the program *CRYSON* (Svergun *et al.*, 1998). The theoretical scattering signal for CorA (PDB entry 2bbj; Lunin *et al.*, 2006) was calculated using *CRYSON* assuming one pentameric complex per disc. The data were normalized in relation to the nanodisc data by exploiting the fact that the absolute forward scattering intensity for a dilute system of particles in solution can be calculated as $I(0) = nV^2(\Delta\rho)^2$, where n is the concentration (mol l^{-1}), V is the partial specific molecular volume of the protein, which is 1.35 g cm^3 (Mylonas & Svergun, 2007), and $\Delta\rho$ is the excess scattering-length density of the (hydrogenated) protein in D_2O, which is 3×10^{10} cm^{-2} (Jacrot, 1976).

3. Results

3.1. The stealth nanodisc system: reaching invisibility

The theoretical deuteration levels required for total 'invisibility' of the nanodisc system differ for the various components of this lipid–protein particle. This results from natural differences in the scattering-length density (SLD) between proteins and phospholipids as well as between the head groups and the fatty-acyl residues of the phospholipid bilayer alone (Engelman & Moore, 1975; Jacrot, 1976). The SLD can be calculated by summing over the scattering lengths of the single atoms in a molecule and dividing by the partial specific molecular volume (Glatter & Kratky, 1982).

A buffer based on 100% D_2O is generally favoured in SANS studies in order to minimize the hydrogen incoherent scattering associated with the use of H_2O (Jacrot, 1976). Consequently, for the stealth membrane-protein carriers, zero contrast in 100% D_2O at all of the SANS-relevant length scales is preferable to minimize both the hydrogen incoherent scattering as well as the coherent signal arising from the carrier molecules (Fig. 1).

For the prototype stealth nanodisc we have chosen a PC-based lipid bilayer together with the membrane scaffold protein MSP1D1 (Nath *et al.*, 2007), as several successful reconstitutions of membrane proteins have previously been reported for this nanodisc system. We used PC composed of mixed acyl unsaturated fatty-acyl residues of 16–18 C atoms in length because these are physiologically the most relevant and therefore are most often chosen as model bilayer lipids for the reconstitution of membrane proteins (van Meer *et al.*, 2008).

For a PC-based bilayer in 100% D_2O we calculated that total matching can be achieved when 78% of the head-group atoms and 92% of the acyl-chain H atoms have been

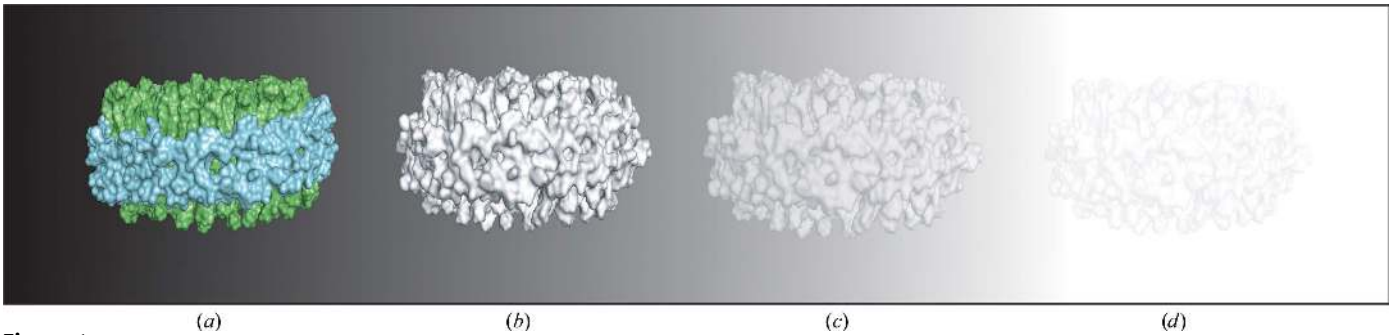

Figure 1
Schematic representation of the stealth nanodisc in buffer solution with a gradually increasing level of D_2O (decreasing greyscale). (*a*) Hydrogenated nanodisc consisting of a phospholipid bilayer (green) and membrane scaffold protein MSP (light blue). (*b*) Stealth nanodisc comprised of deuterated lipid and deuterated MSP at 60% D_2O. (*c*) Stealth nanodisc at 80% D_2O. (*d*) Stealth nanodisc at 100% D_2O.

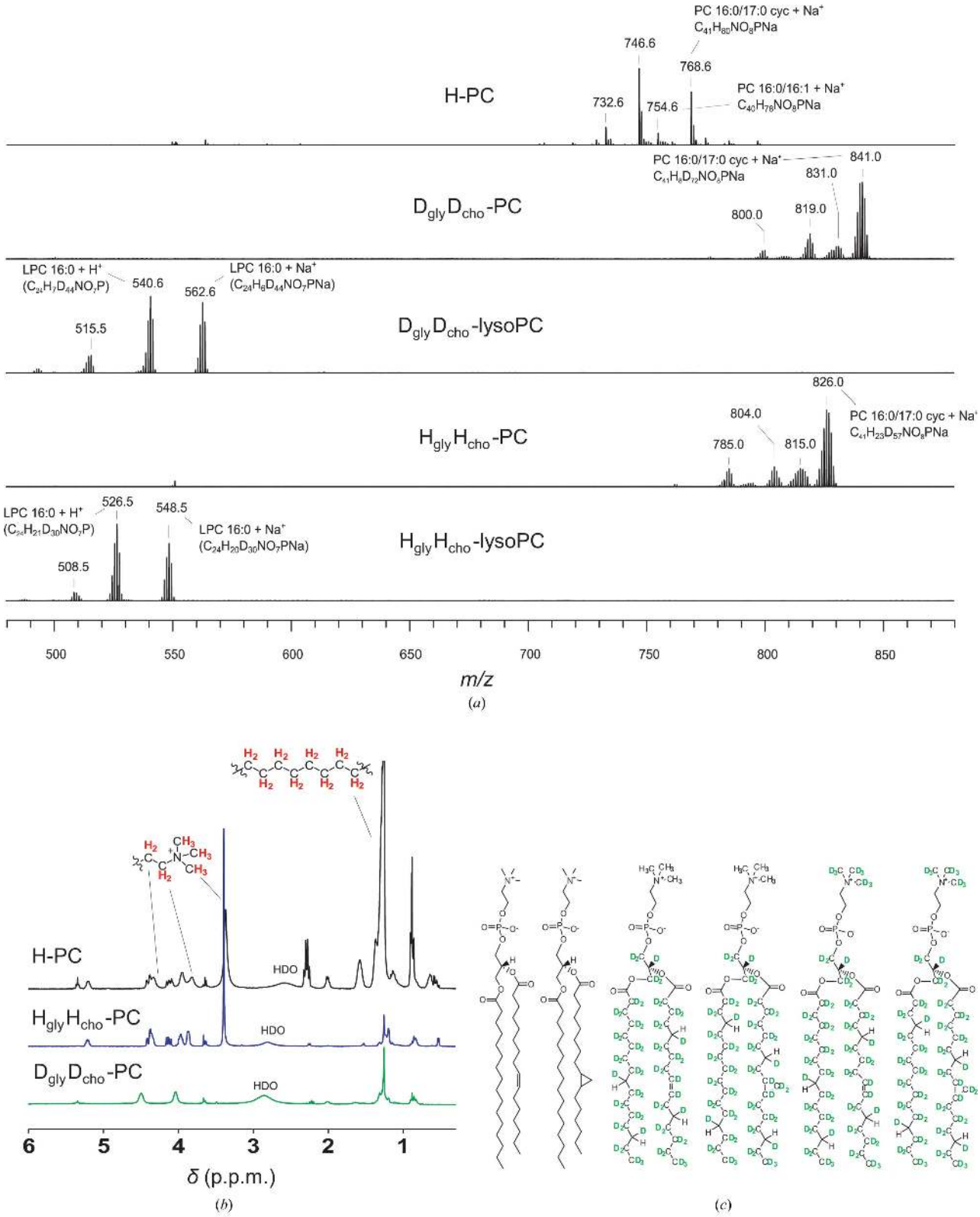

Figure 2
Selective deuteration of phosphatidylcholine in genetically modified *E. coli*. (*a*) Positive-ion MALDI–TOF spectra of purified phosphatidylcholine (PC) obtained from a genetically modified *E. coli* strain grown in hydrogenated medium (trace H-PC), in deuterated medium supplemented with deuterated glycerol and deuterated choline before (trace $D_{gly}D_{cho}$-PC) and after (trace $D_{gly}D_{cho}$-lysoPC) treatment with PLA_2 as well as in deuterated medium supplemented with hydrogenated glycerol and hydrogenated choline before (trace $H_{gly}H_{cho}$-PC) and after (trace $H_{gly}H_{cho}$-lysoPC) treatment with PLA_2. Peaks are marked with their *m*/*z* values and assignments are indicated. (*b*) NMR spectra showing H-PC (black), $H_{gly}H_{cho}$-PC (blue) and $D_{gly}D_{cho}$-PC (green) with HDO representing water traces in the samples. (*c*) Molecular structure of the *E. coli*-produced PC (examples of the main species according to deuteration).

exchanged to deuterium. For the membrane scaffold protein MSP1D1 encircling the bilayer, as for all other proteins, the required level of deuteration is reached when on average 70% of the non-exchangeable H atoms are replaced by D atoms (Engelman & Moore, 1975; Jacrot, 1976; Li *et al.*, 2009). Owing to the exchangeability of the H atoms bound to O, N and S atoms, this leads to an overall level of deuteration of about 75% when the protein is dispersed in 100% D_2O solution.

3.2. Engineering of the stealth-nanodisc components

While several versions of partially deuterated 1-palmitoyl-2-oleoyl-PC and dipalmitoyl-PC (16:0/18:1 and 16:0/16:0, respectively) are commercially available (Bragina & Chupin, 1997), monounsaturated mixed-acyl versions of PC with the specific deuteration levels that would result in stealth properties in 100% D_2O are not. This is because chemical synthesis of these lipids is highly challenging (Bragina & Chupin, 1997). Previous chemical syntheses of deuterated PC have utilized methods that do not allow differentiation between the fatty-acyl residues at positions 1 and 2 of the glycerol (Bragina & Chupin, 1997). Selective deuteration of the head group in unsaturated deuterated phospholipids is accompanied by modifications of the double bonds (de Kruijff *et al.*, 1978). We therefore chose to produce the required PC lipids through biological deuteration in a recently engineered *E. coli* strain (AL95) that produces PC (Bogdanov *et al.*, 2010). *E. coli* may be deuterated to a very high degree (Paliy *et al.*, 2003) and has a very simple lipid composition (Raetz, 1978) compared, for example, with yeast (Kaneko *et al.*, 1976), and was therefore chosen in order to facilitate biosynthesis as well as subsequent extraction and lipid isolation.

Minimal medium was chosen for the production of both deuterated nanodisc components in order to obtain better control of the deuteration levels. For the bacterial lipids we were able to achieve targeted head-group deuteration through the addition of deuterated glycerol, while the deuteration of the acyl chains could be controlled through the total level of D_2O in the growth medium. Also, the addition of commercially available partially deuterated choline chloride retaining a protonated ethylene group (trimethylammonium-d_9) enabled an additional level of control of head-group deuteration. Furthermore, choline supplementation resulted in higher yields of PC, as seen for its hydrogenated analogue (Bogdanov *et al.*, 2010).

The fatty-acyl distribution of *E. coli* phospholipids is dependent on the growth conditions (de Mendoza *et al.*, 1983). For this particular strain, cells harvested in the stationary growth phase resulted in a lipid extract containing 1-palmitoyl-2-palmitoleoyl-*sn*-glycero-3-phosphocholine (16:0/16:1 PC) as shown by positive-ion MALDI–TOF analysis (Fuchs *et al.*, 2010), with *m*/*z* 732.6 and 754.6 corresponding to the proton and sodium adducts, respectively (Fig. 2*a*, trace H-PC). The data also showed the presence of primarily PC with a cyclopropane-modified fatty-acyl residue at *m*/*z* 746.6 and 768.6 (16:0/17:0cyc PC) typical of *E. coli* lipids (Magnuson *et al.*, 1993). These cyclopropanated residues appear to improve stability and are less reactive to oxidative modifications than the corresponding unsaturated fatty-acyl residues, while keeping the overall membrane fluidity unchanged (Law, 1971; Dufourc *et al.*, 1983).

The PC biosynthesized in deuterated medium at ~100% D_2O in the presence of deuterated glycerol and partially deuterated choline chloride (trimethylammonium-d_9) exhibited a narrow distribution of highly deuterated PC with no major changes in the fatty-acyl distribution (Fig. 2*a*, trace $D_{gly}D_{cho}$-PC). The peaks at *m*/*z* 800.0 and 819.0 were assigned to the H^+ adducts of highly deuterated 16:0/16:1 PC and 16:0/17:0cyc PC, respectively, whereas the two peaks at *m*/*z* 831.0 and 841.0 were assigned to the respective Na^+ adducts of the same two species. While the Na^+ adduct of completely deuterated 16:0/17:0cyc PC (d_{80}) should result in *m*/*z* 849.0, the observed lower value of 841.0 for the most abundant species can be explained by incompletely deuterated 16:0/17:0cyc PC with a remaining average of eight H atoms ($C_{41}H_8D_{72}NO_8PNa$). This interpretation was further confirmed through characterization of the PC fraction after digestion with phospholipase PLA_2, an enzyme that selectively cleaves the fatty-acyl residue in the *sn*-2 position (Fuchs *et al.*, 2007). Prior to digestion, the most abundant peak was at *m*/*z* 841.0 and after digestion it was at *m*/*z* 562.6 (Fig. 2*a*, traces $D_{gly}D_{cho}$-PC and $D_{gly}D_{cho}$-lysoPC). Fully deuterated lysoPC 16:0 would give a mass of 568.6 for the Na^+ adduct; however, the lower value of 562.6 observed for the most abundant species can be assigned to a partially deuterated lysoPC containing six H atoms ($C_{24}H_6D_{44}NO_7PNa$). This indicates a loss of two H atoms after the deletion of the fatty-acyl residue in the *sn*-2 position. The biosynthesis approach gave a narrow distribution of deuteration level for PC, with an observed standard deviation of 1.3 atomic mass units (amu) within the single species. When compared with the 80 possible D atoms in the 16:0/17:0cyc PC this corresponds to a ~1.6% deviation in the deuteration level for the overall lipid. The biosynthesis of PC in ~100% D_2O in the presence of protonated carbon sources showed a similar fatty-acyl distribution but with a shift in *m*/*z* from 841.0 to 826.0 (Fig. 2*a*, trace $H_{gly}H_{cho}$-PC). Assuming no change in fatty-acyl distribution, this decrease of 15 amu corresponds well to the difference between the protonated and deuterated carbon sources added to the medium (choline possessing nine and glycerol five H atoms). An exact decrease of 14 amu can be observed when comparing the lyso fractions of both $D_{gly}D_{cho}$-PC and $H_{gly}H_{cho}$-PC subsequent to PLA_2 digestion, with a shift from *m*/*z* 562.6 for a deuterated carbon-source preparation to *m*/*z* 548.5 for a protonated carbon-source preparation (Fig. 2*a*, traces $D_{gly}D_{cho}$-lysoPC and $H_{gly}H_{cho}$-lysoPC), indicating completely hydrogenated head groups in this partially deuterated species.

The localization of the residual H atoms in the two aforementioned deuterated versions of PC was investigated by ^{1}H NMR by comparison to the hydrogenated analogue (Fig. 2*b*). The two signals observed at 4.04 and 4.50 p.p.m. in $D_{gly}D_{cho}$-PC were in agreement with the ethylene H atoms of the choline head group (Fig. 2*b*, trace $D_{gly}D_{cho}$-PC green). Although they were slightly downfield-shifted compared with

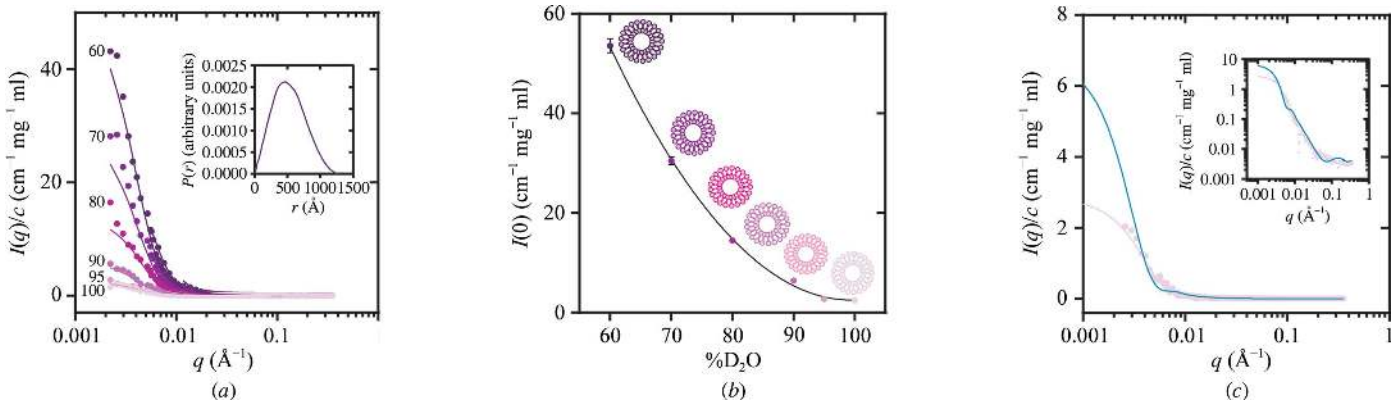

Figure 3
Stealth liposome SANS contrast variation. (*a*) SANS data together with IFT fits showing the decrease in scattering intensity from the stealth liposomes with the indicated increasing levels of D_2O in the buffer. The inset shows the pair distance distribution function for stealth liposomes at 60% D_2O. (*b*) SANS forward scattering as a function of the D_2O content of the buffer. Inset: a schematic representation of stealth liposomes with decreasing contrast in D_2O. (*c*) Stealth liposome SANS data (light purple) and theoretical SANS data calculated for liposomes with commercially available D_{64}-POPC (Avanti Polar Lipids; petrol). The insert shows a comparison of the two versions of deuterated liposomes (light purple and dark cyan) on a logarithmic scale.

the hydrogenated sample, this assignment was confirmed by ^{13}C NMR (65.9 and 60.3 p.p.m., respectively). If these two aforementioned peaks are assumed to correspond to two H atoms each, as is the case for the added choline, this gives a total of approximately four H atoms in the fatty-acyl signal at around 1.2 p.p.m. (Fig. 2*b*, green trace). NMR analysis of $H_{gly}H_{cho}$-PC obtained from *E. coli* grown with hydrogenated carbon sources, as shown in Fig. 2(*b*) (blue), confirmed head-group incorporation of protonated glycerol and choline, while the fatty-acyl residues remained highly deuterated. The glycerol and choline signals between 3.5 and 5.5 p.p.m. were identical to the hydrogenated sample, whereas the acyl signals were similar to the highly deuterated sample. The many small signals observed in NMR for the two deuterated analogues (Fig. 2*b*, blue and green traces) are associated with the acyl residues and indicate that the remaining H atoms were randomly distributed throughout the chains. The combined MALDI–TOF and ^1H NMR data allowed the calculation of the deuteration levels for the most abundant $D_{gly}D_{cho}$-PC species 16:0/17:0cyc PC. For the 18 head-group H atoms present in normal hydrogenated conditions, the remaining four H atoms gave 78% deuteration. For the acyl chains, 58 of the 62 H atoms were exchanged to deuterium, corresponding to 93% deuteration. Fig. 2(*c*) illustrates examples of the most abundant species before and after deuteration.

The stealth version of MSP1D1 with the 'match-out' deuteration level was expressed in *E. coli* BL21 (DE3) cells grown in 85% deuterated minimal medium according to established protocols for protein deuteration (Leiting *et al.*, 1998). The initial yields of the two nanodisc components achieved using this approach were in the region of $\sim$50 mg l^{-1} for deuterated PC and $\sim$25 ml^{-1} for deuterated MSP1D1. These amounts are sufficient for several nanodisc assemblies that can be used in subsequent SAXS and SANS analysis. Based on the amount of cell paste obtained in a pilot fermentation study, this can be scaled up to over 200 mg l^{-1} for PC. A similar scale-up is also expected to be possible for MSP1D1 through fermentation.

3.3. Stealth carrier assembly and SANS contrast variation

Small unilamellar liposomes were prepared from purified $D_{gly}D_{cho}$-PC (Supporting Fig. S1*a*[1]). These stealth liposomes showed an average diameter of 110 nm when probed by dynamic light scattering. The liposome size was also confirmed through SANS, in which model fitting (Kucerka *et al.*, 2004) and the pair distance distribution function, $p(r)$, obtained by indirect Fourier transformation gave a maximum dimension of 120 nm (Fig. 3*a*, insert). Contrast-variation SANS data collected over a broad q-range for the prepared liposomes at increasing D_2O content in the buffer showed a systematic decrease in scattering intensity with increasing level of D_2O (Fig. 3*a*). The minimum in scattering intensity for the liposomes derived from the SANS forward scattering as a function of D_2O content is observed to be close to 100% D_2O (Fig. 3*b*). A comparison of the scattering from the stealth liposomes to the theoretically expected results for the commercially available D_{64}-POPC deuterated lipids in 100% D_2O is provided in Fig. 3(*c*). The plot shows that the forward scattering of the liposomes is minimized in the stealth lipid system. This is expected, as the commercially available D_{64}-POPC lipids are not matched out at 100% D_2O, which is the optimal contrast in order to maximize the signal-to-noise ratio of an inserted membrane protein. However, and more importantly, the oscillation at intermediate to high q that is present in the commercial system owing to the different internal scattering length densities in the lipids is much less visible in the stealth lipids. Since the scattering signal from a typical membrane protein is expected to be present in this region (Fig. 5) this is an important result. Fig. 3(*c*) also shows that while the

[1] Supporting information has been deposited in the IUCr electronic archive (Reference: KW5078).

biosynthetically produced lipids minimize the scattering from the liposomes, the scattering intensity at 100% D_2O is unfortunately not zero. A complete $I(q) = 0$ is impossible to obtain owing to internal deuteration fluctuations within the single lipids. However, the data indicate that an even better match-out could potentially be achieved through further fine-tuning of the growth conditions. This will be pursued in future work.

SAXS analysis of deuterated MSP1D1 on its own showed that the purified amphipathic protein belts formed large disordered aggregates when dissolved in aqueous solution, making subsequent SANS contrast-variation investigations unreliable.

However, by combining the produced $D_{gly}D_{cho}$-PC (Supporting Fig. S1*a*) and deuterated MSP1D1 (Supporting Fig. S1*b*) using standard nanodisc-preparation procedures (Ritchie *et al.*, 2009), successful assembly of nanodiscs was achieved. Size-exclusion chromatography showed an elution profile (Supporting Fig. S1*c*) commonly observed for hydrogenated nanodiscs (Ritchie *et al.*, 2009). A small shoulder observed on the chromatogram indicated that the ratio of phospholipid to membrane-scaffold protein was not at the optimal level for reconstitution. Non-optimal ratios can arise from slight discrepancies in concentration measurements when dealing with deuterated versions of the phospholipids and MSP and would lead to fractions of slightly larger lipid–protein aggregates. Therefore, only the fractions thought to contain nanodiscs of typical size were used for further analysis (Supporting Fig. S1*c*, green). Successful nanodisc assembly was supported by SAXS analysis. The very distinct SAXS curve characteristic of the nanodisc system (Fig. 4*a*, green) gave a $p(r)$ function that indicated a maximum size of approximately 12 nm for the discs. This was consistent with the previously observed size of nanodiscs with attached His tags, which was also the case in this preparation (Skar-Gislinge *et al.*, 2010). Finally, a recently derived mathematical model of the nanodisc (Skar-Gislinge *et al.*, 2010; Skar-Gislinge & Arleth, 2011) was fitted to the experimental data (Fig. 4*a*, black) and confirmed that the SAXS data were fully consistent with the nanodiscs having approximately the same structure as has previously been observed by our group (Skar-Gislinge *et al.*, 2010; Skar-Gislinge & Arleth, 2011).

The SANS contrast-variation study of the stealth nanodisc showed a systematic decrease in scattering intensity with an increasing level of deuterium in the solvent and revealed a clear minimum in the overall scattering intensity at 100% D_2O (Figs. 4*b* and 4*c*). This initial preparation of the stealth carriers resulted in a small residual signal for both the stealth liposomes and the nanodiscs. This could be owing to the aforementioned statistical fluctuations in the deuteration of the lipids and the MSP1D1. The observed intensity decreased to a level only slightly above that of the experimental background and was therefore difficult to measure accurately. In Fig. 4(*d*) we compare the residual nanodisc signal with the SANS signal of a nanodisc assembled with D-MSP1D1 in combination with commercially available chemically synthesized D_{64}-POPC (Avanti Polar Lipids) containing fully deuterated fatty-acyl chains and protonated head groups. While the forward scattering signals from both of the deuterated nanodisc samples are over ∼150-fold lower than that of a protonated nanodisc (Fig. 4*d*, inset), the biosynthesized stealth nanodisc clearly shows an improvement, with a lowered

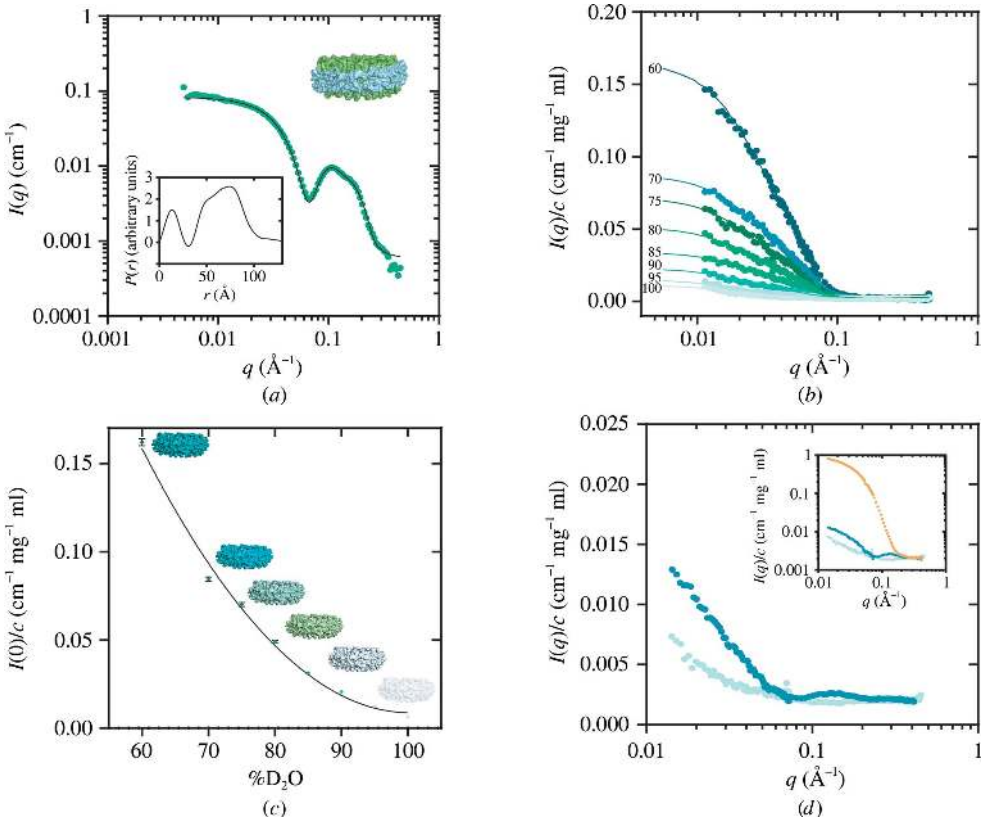

Figure 4
Stealth nanodisc assembly and SANS contrast variation. (*a*) Small-angle X-ray scattering data from nanodiscs in H_2O (green) shown together with the fitted structural model (black). The inset shows the pair distance distribution function for the stealth discs with information about the disc size. (*b*) SANS data together with IFT fits showing the decrease in scattering intensity from the stealth nanodiscs with the indicated increasing buffer content of D_2O in solution. (*c*) SANS forward scattering as a function of the D_2O content of the buffer. (*d*) Stealth nanodisc SANS data (light green) and SANS data measured for nanodiscs assembled with D-MSP1D1 and commercially available D_{64}-POPC (Avanti Polar Lipids; petrol). The inset shows a comparison of the two versions of deuterated discs (light green and blue) with a protonated version of the nanodisc (orange) on a logarithmic scale.

scattering intensity in the entire q-range when compared with the chemically synthesized version of the disc. An even better match-out could potentially be achievable through further optimization of the deuteration levels of both the lipid bilayer and the membrane-scaffold protein.

In order to obtain insight into the potential performance of the developed stealth nanodiscs, a comparison of the residual stealth nanodisc signal was performed with a range of possible protein targets of different sizes (Fig. 5), where the theoretical scattering intensity was generated using the program *CRYSON* (Svergun *et al.*, 1998). For EGFR, for which the complete structure has yet to be resolved, the scattering data were based on a manual assembly of the available structural parts (Zhang *et al.*, 2006; Ferguson *et al.*, 2003; Bocharov *et al.*, 2008; Ogiso *et al.*, 2002; Montelione *et al.*, 1992), while for the other proteins the curves were generated using already available structural information (Palczewski *et al.*, 2000; Shintre *et al.*, 2013; Pedersen *et al.*, 2007; Shinoda *et al.*, 2009; Higgins *et al.*, 2004). For larger protein complexes such as EGFR with one active dimer per nanodisc, a ∼120-fold larger forward scattering intensity could be observed for the protein compared with the stealth nanodisc carrier, while for the CorA pentameric complex (Lunin *et al.*, 2006) the signal is ∼45-fold larger than that of the stealth nanodisc. In such cases the signal from the nanodisc can be ignored to the first order, allowing the use of the stealth nanodisc system in combination with already tested bead-modelling and rigid-body approaches (Svergun, 1999; Svergun *et al.*, 2001) to obtain a good low-resolution determination of the membrane-protein structure. In the case of smaller membrane-protein systems, it will be beneficial to include a primitive model of the weakly scattering stealth nanodisc in order to resolve the membrane-protein signal. In all cases, combining the bead-modelling approach with an approximate model of the weakly scattering stealth nanodisc should make it possible to further improve the structural resolution of the membrane protein towards the standard ∼10 Å resolution that is typically achievable from small-angle scattering data.

4. Discussion

We have shown that the deuteration level of physiologically relevant PC can be separately controlled for head groups and tails *via* a biosynthetic pathway. This includes targeted substitution of hydrogen by deuterium in the different parts of the phospholipid molecule through systematic addition of deuterated nutrients during biosynthesis. We have exploited this to prepare an advanced carrier system for membrane proteins that becomes 'invisible' to neutrons in 100% D_2O-based buffers. This development offers a general approach to determine the low-resolution structure of membrane proteins and their complexes in solution using already established SAXS/SANS data-analysis methods (Petoukhov & Svergun, 2012; Blanchet & Svergun, 2013).

Using this approach, the deuterated stealth carriers can be produced in sufficiently large amounts to facilititate SANS-based structural studies of membrane proteins that are generally only available in small quantities (Midgett & Madden, 2007; Tate, 2010).

The SAXS analysis of the prepared nanodiscs showed that the overall disc structure did not change compared with POPC nanodiscs that have been described previously (Skar-Gislinge *et al.*, 2010; Skar-Gislinge & Arleth, 2011). This confirmed that the cyclopropane substitution of some of the double bonds in the PC unsaturated fatty-acyl chain that occurs in *E. coli* during the stationary growth phase (Magnuson *et al.*, 1993) and which should not affect the bilayer fluidity (Dufourc *et al.*, 1983) also did not affect nanodisc formation. Harvesting cells in this growth phase is therefore recommended as it leads to the highest biomass and consequently the highest yield of phospholipid for the lowest cost of deuterated medium. The fatty-acyl distribution can be regulated during the bacterial growth cycle (Magnuson *et al.*, 1993), creating additional opportunities for the development of these stealth lipids.

The deuteration approach through biosynthesis also allows the production of different types of specifically deuterated physiologically relevant PCs that may be exploitable using other structural techniques such as NMR and neutron reflectometry. In NMR studies of complex protein–lipid systems a complete cancellation of the ^{1}H signal through the use of fully deuterated PC leads to significant simplification in data analysis (Hagn *et al.*, 2013), while physiologically relevant PC may provide better stability of the incorporated membrane protein (van Meer *et al.*, 2008). In neutron reflectometry, on the other hand, the advantages lie in obtaining different contrasts in different parts of the lipid bilayer, which can be controlled through different deuteration levels, thus highlighting specific parts (Majewski *et al.*, 2000). This can then be exploited not only in studies of the effect of the lipid environment on membrane-protein systems but also in studies of

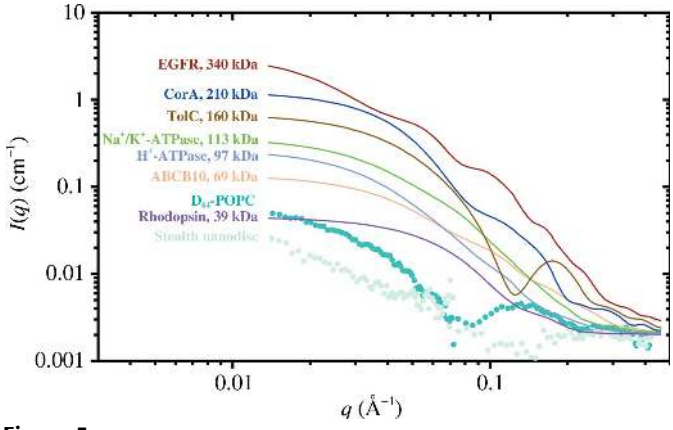

Figure 5
Comparison of the stealth nanodisc SANS signal with those of model proteins. SANS data from stealth nanodiscs in 100% D_2O (green) and D_{64}-POPC nanodiscs (petrol) shown together with the theoretical scattering signals for bovine rhodopsin (purple), ATP-binding cassette transporter (ABCB10; orange), H^+-ATPase (light blue), Na^+/K^+-ATPase (green), trimeric TolC protein from *E. coli* (brown), bacterial magnesium transporter CorA (dark blue) and the epidermal growth factor receptor EGFR (dark red). All scattering curves were generated using *CRYSON* and PDB entries available for each protein (PDB entries 1f88, 4ayw, 3b8c, 2zxe, 1tqq and 2bbj), while the EGFR structure was combined in *PyMOL* (http://www.pymol.org) using PDB entries 1ivo, 1nql, 2jwa, 2gs6 and 1egf.

various ligands and potential drugs and their interactions with the membrane (Akesson *et al.*, 2012). In this context, using the lipids to understand, for example, the interactions of antimicrobial peptides with bacterial membranes could lead to novel insights into the increasing problem of antibiotic resistance in bacteria (Molloy, 2010).

In the case of the reported stealth nanodiscs and liposomes, a residual signal is visible for both carriers when investigated by SANS in 100% D_2O. This signal is negligible by comparison with that of a possible protein signal in 100% D_2O, as shown in the comparison of the nanodisc carrier with a range of model membrane-protein signals. In these examples, the signal caused by the nanodisc can to a good approximation be ignored when reconstructing the low-resolution membrane-protein structure from SANS data. However, for studies of small membrane proteins with a size of ∼50 kDa, for which the membrane-protein signal is also relatively weak in 100% D_2O, the residual nanodisc signal needs either to be incorporated in the data analysis or needs further reduction to achieve the same negligibility.

Stealth liposomes naturally give a larger residual signal than the nanodiscs owing to the much larger size of the particles. However, they can be used as an alternative carrier for larger membrane-protein systems where reconstitution into nanodiscs is not appropriate or where a more cell-like environment is desired, for example in electrolyte or pH-gradient studies.

For accurate and reliable data interpretation in terms of the structural parameters, the scattering data should be obtained from a pure and well defined sample, as with any other systems studied by SAS. As with regular nanodiscs, the reconstitution conditions should be optimized for each membrane protein under study (Ritchie *et al.*, 2009). Based on the initial stealth nanodisc assembly shown in this article, we do not foresee that the reconstitution conditions will differ significantly for these specifically deuterated nanodiscs. The use of D_2O-based buffer in SANS can in unfavourable cases give rise to greater protein instability (Makhatadze *et al.*, 1995), that may compromise the SANS data quality.

Nevertheless, for membrane-protein complexes the nanodisc-based approach of 'mimicked solubility' has already led to an improved understanding of membrane-protein function in a more native-like environment (Ritchie *et al.*, 2009) as well as structure, using for example NMR (Hagn *et al.*, 2013). We therefore anticipate that both the stealth nanodiscs as well as the stealth liposomes will be a great advantage as 'neutron-invisible' carriers to be used as a platform for SANS structural studies of membrane proteins in solution. Combined with the advancement of *ab initio* and rigid-body modelling programs for structural data analysis and the development of powerful next-generation neutron sources, data obtained through this development may lead to further insights into the dynamics, protein–ligand binding and conformational changes of membrane proteins in a solution environment. Collectively, this approach establishes an experimental basis for using the system for low-resolution structural studies of membrane proteins using the same data-analysis tools as are already available for soluble proteins in solution (Konarev *et al.*, 2006; Petoukhov & Svergun, 2012; Blanchet & Svergun, 2013).

The authors gratefully acknowledge the access to the large-scale facility SANS and SAXS beamtime at SANS beamline KWS1 at Forschungs Neutronenquelle Heinz Maier-Leibnitz (FRM II), Munich, SANS beamline D11 at the Institut Laue–Langevin (ILL), Grenoble, the BM29 Bio-SAXS beamline at the European Synchrotron Radiation Facility (ESRF), Grenoble and the Deuteration Laboratory PSB platform operated together with the ILL Life Sciences Group, Grenoble. In particular, the authors would like to thank Dr Adam Round, Dr Petra Pernot and Dr Ralph Schweins for beamline support in Grenoble. The authors also wish to thank Professor William Dowhan and his group at the University of Texas, USA for their kind contribution in providing the PC-producing *E. coli* strain. The authors would like to thank Martin Cramer Pedersen for help with model calculation data and Professor Birger Lindberg Møller for critical reading of the manuscript. Finally, we thank the European Spallation Source and the Danish Government-funded UNIK Synthetic Biology program for co-funding of the project as well as the Danish Research Council-funded DanScatt organization for providing financial support for travel to the large-scale facility SAXS and SANS beamlines. JS thanks the German Research Council for financial support (SFB 1052/B6). VTF acknowledges support from the UK Engineering and Physical Sciences Research Council (EPSRC) for the ILL Deuteration Laboratory under grants GR/R99393/01 and EP/C015452/1, from the EU NMI3 programme under FP7 and also through the EU CRISP programme (grant No. 283745).

References

Akesson, A., Lind, T. K., Barker, R., Hughes, A. & Cardenas, M. (2012). *Langmuir*, **28**, 13025–13033.
Andersen, H. D., Wang, C., Arleth, L., Peters, G. H. & Westh, P. (2011). *Proc. Natl Acad. Sci. USA*, **108**, 1874–1878.
Artero, J.-B., Härtlein, M., McSweeney, S. & Timmins, P. (2005). *Acta Cryst.* D**61**, 1541–1549.
Baker, M. (2010). *Nature (London)*, **465**, 823–826.
Bayburt, T. H., Grinkova, Y. V. & Sligar, S. G. (2002). *Nano Lett.* **2**, 853–856.
Berthaud, A., Manzi, J., Pérez, J. & Mangenot, S. (2012). *J. Am. Chem. Soc.* **134**, 10080–10088.
Bhattacharya, A. (2009). *Nature (London)*, **459**, 24–27.
Blanchet, C. E. & Svergun, D. I. (2013). *Annu. Rev. Phys. Chem.* **64**, 37–54.
Bligh, E. G. & Dyer, W. J. (1959). *Can. J. Biochem. Physiol.* **37**, 911–917.
Bocharov, E. V., Mineev, K. S., Volynsky, P. E., Ermolyuk, Y. S., Tkach, E. N., Sobol, A. G., Chupin, V. V., Kirpichnikov, M. P., Efremov, R. G. & Arseniev, A. S. (2008). *J. Biol. Chem.* **283**, 6950–6956.
Bogdanov, M., Heacock, P., Guan, Z. & Dowhan, W. (2010). *Proc. Natl Acad. Sci. USA*, **107**, 15057–15062.
Bragina, N. A. & Chupin, V. V. (1997). *Russ. Chem. Rev.* **66**, 975–986.
Calcutta, A., Jessen, C. M., Behrens, M. A., Oliveira, C. L., Renart, M. L., González-Ros, J. M., Otzen, D. E., Pedersen, J. S., Malmendal, A. & Nielsen, N. C. (2012). *Biochim. Biophys. Acta*, **1818**, 2290–2301.
Chan, Y.-H. M. & Boxer, S. G. (2007). *Curr. Opin. Chem. Biol.* **11**, 581–587.

Cherezov, V., Rosenbaum, D. M., Hanson, M. A., Rasmussen, S. G., Thian, F. S., Kobilka, T. S., Choi, H. J., Kuhn, P., Weis, W. I., Kobilka, B. K. & Stevens, R. C. (2007). *Science*, **318**, 1258–1265.

Dufourc, E. J., Smith, I. C. & Jarrell, H. C. (1983). *Chem. Phys. Lipids*, **33**, 153–177.

Engelman, D. M. & Moore, P. B. (1975). *Annu. Rev. Biophys. Bioeng.* **4**, 219–241.

Fagerberg, L., Jonasson, K., von Heijne, G., Uhlén, M. & Berglund, L. (2010). *Proteomics*, **10**, 1141–1149.

Ferguson, K. M., Berger, M. B., Mendrola, J. M., Cho, H.-S., Leahy, D. J. & Lemmon, M. A. (2003). *Mol. Cell*, **11**, 507–517.

Fuchs, B., Müller, K., Göritz, F., Blottner, S. & Schiller, J. (2007). *Lipids*, **42**, 991–998.

Fuchs, B., Süss, R. & Schiller, J. (2010). *Prog. Lipid Res.* **49**, 450–475.

Glatter, O. (1977). *J. Appl. Cryst.* **10**, 415–421.

Glatter, O. & Kratky, O. (1982). *Small Angle X-ray Scattering*. New York: Academic Press.

Hagn, F., Etzkorn, M., Raschle, T. & Wagner, G. (2013). *J. Am. Chem. Soc.* **135**, 1919–1925.

Higgins, M. K., Eswaran, J., Edwards, P., Schertler, G. F., Hughes, C. & Koronakis, V. (2004). *J. Mol. Biol.* **342**, 697–702.

Hunt, J. F., McCrea, P. D., Zaccaï, G. & Engelman, D. M. (1997). *J. Mol. Biol.* **273**, 1004–1019.

Hura, G. L., Menon, A. L., Hammel, M., Rambo, R. P., Poole, F. L. II, Tsutakawa, S. E., Jenney, F. E. Jr, Classen, S., Frankel, K. A., Hopkins, R. C., Yang, S., Scott, J. W., Dillard, B. D., Adams, M. W. W. & Tainer, J. A. (2009). *Nature Methods*, **6**, 606–612.

Jacques, D. A., Guss, J. M., Svergun, D. I. & Trewhella, J. (2012). *Acta Cryst.* D**68**, 620–626.

Jacques, D. A. & Trewhella, J. (2010). *Protein Sci.* **19**, 642–657.

Jacrot, B. (1976). *Rep. Prog. Phys.* **39**, 911–953.

Kaneko, H., Hosohara, M., Tanaka, M. & Itoh, T. (1976). *Lipids*, **11**, 837–844.

Konarev, P. V., Petoukhov, M. V., Volkov, V. V. & Svergun, D. I. (2006). *J. Appl. Cryst.* **39**, 277–286.

Kruijff, B. de, van Zoelen, E. J. & van Deenen, L. L. (1978). *Biochim. Biophys. Acta*, **509**, 537–542.

Kucerka, N., Nagle, J. F., Feller, S. E. & Balgavý, P. (2004). *Phys. Rev. E Stat. Nonlin. Soft Matter Phys.* **69**, 051903.

Law, J. H. (1971). *Acc. Chem. Res.* **4**, 199–203.

Leiting, B., Marsilio, F. & O'Connell, J. F. (1998). *Anal. Biochem.* **265**, 351–355.

Li, J., Callaway, D. J. & Bu, Z. (2009). *J. Mol. Biol.* **392**, 166–180.

Lunin, V. V., Dobrovetsky, E., Khutoreskaya, G., Zhang, R., Joachimiak, A., Doyle, D. A., Bochkarev, A., Maguire, M. E., Edwards, A. M. & Koth, C. M. (2006). *Nature (London)*, **440**, 833–837.

Magnuson, K., Jackowski, S., Rock, C. O. & Cronan, J. E. Jr (1993). *Microbiol. Rev.* **57**, 522–542.

Majewski, J., Kuhl, T. L., Wong, J. Y. & Smith, G. S. (2000). *J. Biotechnol.* **74**, 207–231.

Makhatadze, G. I., Clore, G. M. & Gronenborn, A. M. (1995). *Nature Struct. Biol.* **2**, 852–855.

Meer, G. van, Voelker, D. R. & Feigenson, G. W. (2008). *Nature Rev. Mol. Cell Biol.* **9**, 112–124.

Mendoza, D. de, Klages Ulrich, A. & Cronan, J. E. (1983). *J. Biol. Chem.* **258**, 2098–2101.

Midgett, C. R. & Madden, D. R. (2007). *J. Struct. Biol.* **160**, 265–274.

Molloy, S. (2010). *Nature Rev. Genet.* **11**, 240.

Montelione, G. T., Wüthrich, K., Burgess, A. W., Nice, E. C., Wagner, G., Gibson, K. D. & Scheraga, H. A. (1992). *Biochemistry*, **31**, 236–249.

Mylonas, E. & Svergun, D. I. (2007). *J. Appl. Cryst.* **40**, s245–s249.

Nath, A., Atkins, W. M. & Sligar, S. G. (2007). *Biochemistry*, **46**, 2059–2069.

Ogiso, H., Ishitani, R., Nureki, O., Fukai, S., Yamanaka, M., Kim, J.-H., Saito, K., Sakamoto, A., Inoue, M., Shirouzu, M. & Yokoyama, S. (2002). *Cell*, **110**, 775–787.

Palczewski, K., Kumasaka, T., Hori, T., Behnke, C. A., Motoshima, H., Fox, B. A., Le Trong, I., Teller, D. C., Okada, T., Stenkamp, R. E., Yamamoto, M. & Miyano, M. (2000). *Science*, **289**, 739–745.

Paliy, O., Bloor, D., Brockwell, D., Gilbert, P. & Barber, J. (2003). *J. Appl. Microbiol.* **94**, 580–586.

Pedersen, B. P., Buch-Pedersen, M. J., Morth, J. P., Palmgren, M. G. & Nissen, P. (2007). *Nature (London)*, **450**, 1111–1114.

Pedersen, J. S., Hansen, S. & Bauer, R. (1994). *Eur. Biophys. J.* **22**, 379–389.

Pedersen, J. S., Posselt, D. & Mortensen, K. (1990). *J. Appl. Cryst.* **23**, 321–333.

Pernot, P., Round, A., Theveneau, P., Giraud, T., Nogueira-Fernandes, R., Nurrizzo, D., Spruce, D., Surr, J., McSweeney, S., Felisaz, F., Foedinger, L., Gobbo, A., Huet, J., Villard, C. & Cipriani, F. (2010). *J. Phys. Conf. Ser.* **247**, 012009.

Petkovic, M., Schiller, J., Müller, M., Benard, S., Reichl, S., Arnold, K. & Arnhold, J. (2001). *Anal. Biochem.* **289**, 202–216.

Petoukhov, M. V. & Svergun, D. I. (2012). *Int. J. Biochem. Cell Biol.* **45**, 429–437.

Pipich, V. (2007). *QtiKWS*. http://iffwww.iff.kfa-juelich.de/~pipich/dokuwiki/doku.php/qtikws.

Pocanschi, C. L., Dahmane, T., Gohon, Y., Rappaport, F., Apell, H. J., Kleinschmidt, J. H. & Popot, J. L. (2006). *Biochemistry*, **45**, 13954–13961.

Raetz, C. R. (1978). *Microbiol. Rev.* **42**, 614–659.

Rambo, R. P. & Tainer, J. A. (2013). *Annu. Rev. Biophys.* **42**, 415–441.

Rasmussen, S. G. F., Choi, H.-J. *et al.* (2011). *Nature (London)*, **469**, 175–180.

Rasmussen, S. G. F., Choi, H.-J., Rosenbaum, D. M., Kobilka, T. S., Thian, F. S., Edwards, P. C., Burghammer, M., Ratnala, V. R., Sanishvili, R., Fischetti, R. F., Schertler, G. F., Weis, W. I. & Kobilka, B. K. (2007). *Nature (London)*, **450**, 383–387.

Rasmussen, S. G. F., DeVree, B. T. *et al.* (2011). *Nature (London)*, **477**, 549–555.

Ritchie, T. K., Grinkova, Y. V., Bayburt, T. H., Denisov, I. G., Zolnerciks, J. K., Atkins, W. M. & Sligar, S. G. (2009). *Methods Enzymol.* **464**, 211–231.

Rochel, N., Ciesielski, F., Godet, J., Moman, E., Roessle, M., Peluso-Iltis, C., Moulin, M., Haertlein, M., Callow, P., Mély, Y., Svergun, D. I. & Moras, D. (2011). *Nature Struct. Mol. Biol.* **18**, 564–570.

Rosenbaum, D. M., Cherezov, V., Hanson, M. A., Rasmussen, S. G. F., Thian, F. S., Kobilka, T. S., Choi, H.-J., Yao, X.-J., Weis, W. I., Stevens, R. C. & Kobilka, B. K. (2007). *Science*, **318**, 1266–1273.

Roth, B. L. & Marshall, F. H. (2012). *Nature (London)*, **492**, 57.

Round, A. R., Franke, D., Moritz, S., Huchler, R., Fritsche, M., Malthan, D., Klaering, R., Svergun, D. I. & Roessle, M. (2008). *J. Appl. Cryst.* **41**, 913–917.

Rouser, G., Siakotos, A. N. & Fleischer, S. (1966). *Lipids*, **1**, 85–86.

Schiller, J., Süss, R., Arnhold, J., Fuchs, B., Lessig, J., Müller, M., Petković, M., Spalteholz, H., Zschörnig, O. & Arnold, K. (2004). *Prog. Lipid Res.* **43**, 449–488.

Shinoda, T., Ogawa, H., Cornelius, F. & Toyoshima, C. (2009). *Nature (London)*, **459**, 446–450.

Shintre, C. A. *et al.* (2013). *Proc. Natl Acad. Sci. USA*, **110**, 9710–9715.

Skar-Gislinge, N. & Arleth, L. (2011). *Phys. Chem. Chem. Phys.* **13**, 3161–3170.

Skar-Gislinge, N., Simonsen, J. B., Mortensen, K., Feidenhans'l, R., Sligar, S. G., Lindberg Møller, B., Bjørnholm, T. & Arleth, L. (2010). *J. Am. Chem. Soc.* **132**, 13713–13722.

Stuhrmann, H. (1982). *Small-angle X-ray Scattering*, edited by O. Glatter & O. Kratky, pp. 197–213. New York: Academic Press.

Svergun, D. I. (1999). *Biophys. J.* **76**, 2879–2886.

Svergun, D. I., Petoukhov, M. V. & Koch, M. H. J. (2001). *Biophys. J.* **80**, 2946–2953.

Svergun, D. I., Richard, S., Koch, M. H. J., Sayers, Z., Kuprin, S. & Zaccai, G. (1998). *Proc. Natl Acad. Sci. USA*, **95**, 2267–2272.

Tate, C. G. (2010). *Methods Mol. Biol.* **601**, 187–203.

Terstappen, G. C. & Reggiani, A. (2001). *Trends Pharmacol. Sci.* **22**, 23–26.
Toft, K. N., Vestergaard, B., Nielsen, S. S., Snakenborg, D., Jeppesen, M. G., Jacobsen, J. K., Arleth, L. & Kutter, J. P. (2008). *Anal. Chem.* **80**, 3648–3654.
White, S. H. (2009). *Nature (London)*, **459**, 344–346.
White, T., Bursten, S., Federighi, D., Lewis, R. A. & Nudelman, E. (1998). *Anal. Biochem.* **258**, 109–117.
Xia, Y., Lu, L. J. & Gerstein, M. (2006). *J. Mol. Biol.* **357**, 339–349.
Zhang, X., Gureasko, J., Shen, K., Cole, P. A. & Kuriyan, J. (2006). *Cell*, **125**, 1137–1149.